Johann Radon Institute for
Computational and Applied Mathematics
Austrian Academy of Sciences (ÖAW)

Two finite element methods on hybrid meshes and their applications to the fluid-structure interaction problems

H. Yang

RICAM-Report 2011-24

Two finite element methods on hybrid meshes and their applications to the fluid-structure interaction problems

Huidong Yang[a,1]

[a] *Austrian Academy of Sciences,*
Johann Radon Institute for Computational and Applied Mathematics,
Science Park, Building B, Altenberger Strasse 69, 4040 Linz, Austria

Abstract

Two finite element methods on hybrid meshes containing tetrahedral, pyramidic, prismatic and hexahedral elements are considered. The first method is based on a conforming subdivision of pyramids, prisms and hexahedra into pure tetrahedra without introducing any new node, namely, in a pure geometrical way. The second one is constructed by a conforming subdivision of pyramids, prisms and hexahedra into pure tetrahedra with new nodes on the quadrilateral face centers and on the non-tetrahedral volume centers, where each introduced additional nodal degree of freedom is eliminated by local averaging over those degrees of freedom associated to its original neighbouring nodes, namely, in an algebraic way. Both methods preserve the same number of nodal degrees of freedom as the number of original nodes of the hybrid mesh. The methods are used and compared with each other in the finite element discretization of the structure and fluid sub-problems which appear in partitioned algorithms for solving the fluid-structure interaction problems.

Keywords: finite element method, hybrid mesh, conforming mesh, P_1 element, extended linear element, fluid-structure interaction, partitioned algorithm
2010 MSC: 37M05, 65N30, 74F10

[1] huidong.yang@oeaw.ac.at

1. Introduction

Hybrid meshes have appeared in many applications, e.g., see [4, 11] in the computational fluid dynamics. Constructing finite elements on such hybrid meshes is a nontrivial task. In this note, we consider two finite element methods applicable to the hybrid meshes containing four types of elements: tetrahedron, pyramid, prism and hexahedron.

The first finite element is a standard P_1 element constructed on the conforming subdivision of pyramids, prisms and hexahedra into pure tetrahedra without introducing any new node. Such a subdivision method turns out to be fully local without any communication with neighbouring elements. Thus it is efficient and robust to implement in an element-wise manner except that special care has to be taken into account due to different splitting possibilities for each non-tetrahedral element (for other types of polyhedral elements, there may exist many splitting possibilities). This is resolved by splitting each quadrilateral face into two triangles with the diagonal line going through the node with the smallest (or largest) identifier (e.g. global nodal numbering) on that face. Then for each non-tetrahedral element it has very limited subdivision possibilities which could be tabularized.

The second finite element is an extended linear element on hybrid meshes. For this we first make a conforming subdivision of pyramids, prisms and hexahedra into pure tetrahedra by splitting each quadrilateral face into four triangles with added quadrilateral face center node and then in each non-tetrahedral element connecting the original nodes and the new face center nodes with its added volume center node. Afterwards, we take the standard P_1 finite element on the tetrahedral subdivision and substitute the nodal degrees of freedom associated to the added nodes by averaging over neighbouring nodes of the original hybrid mesh. Each resulting nodal basis function turns out to be a weighted linear combination of the standard P_1 basis functions on the subdivision, with larger support.

The reminder of this paper is organized in the following way. In Section 2, we describe how to construct the standard P_1 element on the conforming subdivision of a hybrid mesh. Section 3 deals with the extended linear finite element on a hybrid mesh. Finally, in Section 4, a few numerical results on the fluid-structure interaction (FSI) problem with these two finite elements on hybrid meshes and the comparison of their performance are presented.

2. The P_1 finite element on the conforming subdivision of a hybrid mesh

Let $\mathcal{M}_h$ be an admissible triangulation of a computational domain Ω into tetrahedral, pyramidic, prismic and hexahedral elements (see Fig. 1), i.e. any two elements from $\mathcal{M}_h$ either have no intersection, or have a common node, or have a common edge, or have a common face.

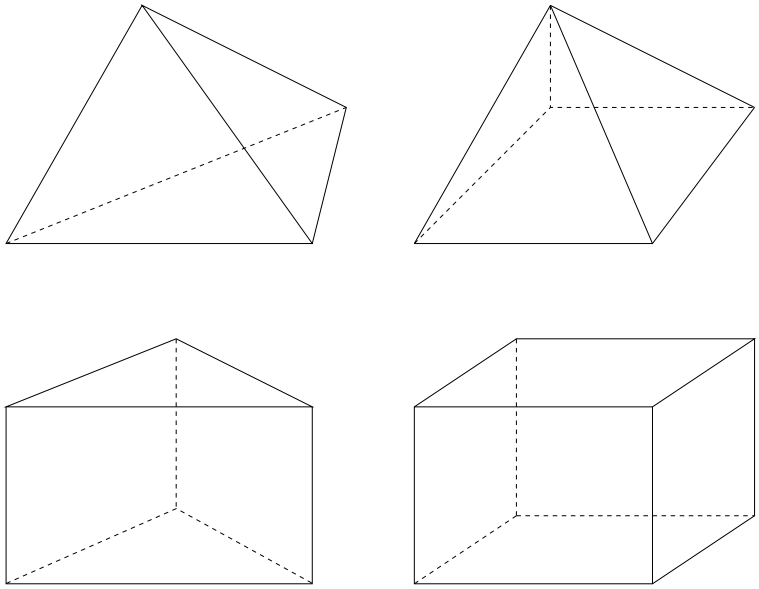

Figure 1: Hybrid elements

2.1. Conforming subdivision of a hybrid mesh without additional nodes

As is known, arbitrary splitting of quadrilateral faces into two triangles may lead to discontinuities across element faces, resulting in non-conforming meshes. On the other hand the subdivision of some elements into tetrahedra may require additional nodes. However, for the first finite element method, we need to preserve the conformity of the subdivided tetrahedral mesh without introducing new nodes. This procedure is performed in the following two steps.

First, let nodal numbering be an identifier of each node. We split each quadrilateral face into two triangles by connecting the diagonal including the node with the smallest identifier from the four nodes on this face, which keeps the subdivision conforming across element faces. See Fig. 2, where the

face $V_1V_2V_3V_4$ is split into two triangles $V_1V_2V_3$ and $V_1V_3V_4$, or $V_1V_2V_4$ and $V_2V_3V_4$.

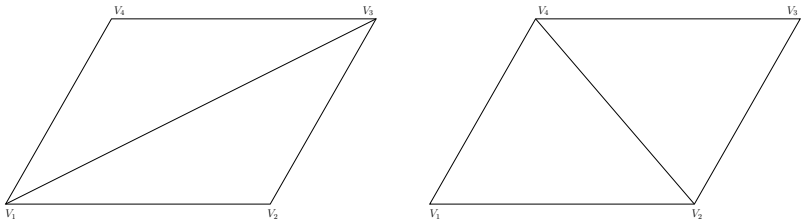

Figure 2: A schematic representation of two subdivisions of a quadrilateral face into triangles: V_1 or V_3 has the smallest identifier on the face $V_1V_2V_3V_4$ (left), V_2 or V_4 has the smallest identifier on the face $V_1V_2V_3V_4$ (right).

Second, we verify that further subdivisions of pyramids, prisms and hexahedra into tetrahedra only require proper local nodal connections inside each element. So no new nodes are added during this step.

2.1.1. Pyramid

According to the first step, the quadrilateral face $V_1V_2V_3V_4$ is split into two triangles by connecting two nodes V_1 and V_3 if V_1 or V_3 has the smallest identifier on face $V_1V_2V_3V_4$, or by connecting two nodes V_2 and V_4 if V_2 or V_4 has the smallest identifier on face $V_1V_2V_3V_4$. See Fig. 3.

The subdivision results for each case are listed in Table 1.

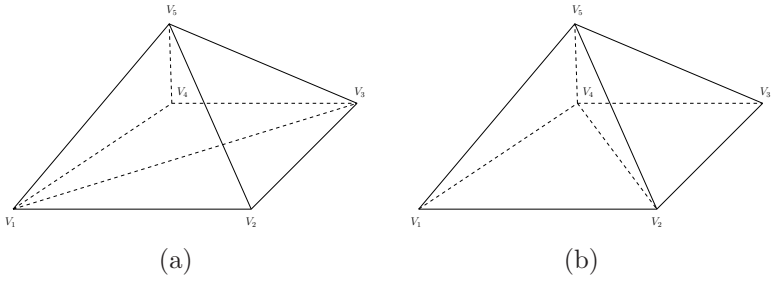

Figure 3: A schematic representation of subdivisions of a pyramid into two tetrahedra.

Without loss of generality, from now on, for each prism and hexahedron, we always assume that the low front left node has the smallest identifier of this element.

Cases	Subdivisions
Fig. 3(a)	$V_1V_2V_3V_5$, $V_1V_3V_4V_5$
Fig. 3(b)	$V_1V_2V_4V_5$, $V_2V_3V_4V_5$

Table 1: Subdivisions of a pyramid.

2.1.2. Prism

According to the first step, faces $V_1V_2V_5V_4$ and $V_1V_3V_6V_4$ are split into triangles by diagonal lines V_1V_5 and V_1V_6, respectively. Depending on the identifiers of V_2, V_3, V_5 and V_6, only two possibilities forming the subdivision remain. See Fig. 4.

The subdivision results for each case are listed in Table 2.

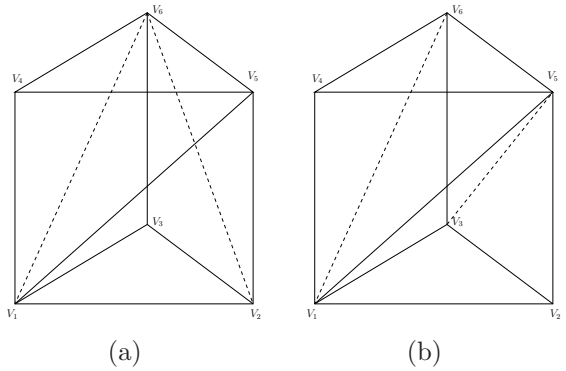

Figure 4: A schematic representation of subdivisions of a prism into three tetrahedra.

Cases	Subdivisions
Fig. 4(a)	$V_1V_2V_5V_6$, $V_1V_2V_3V_6$, $V_1V_4V_5V_6$
Fig. 4(b)	$V_1V_2V_3V_5$, $V_1V_3V_5V_6$, $V_1V_4V_5V_6$

Table 2: Subdivisions of a prism.

2.1.3. Hexahedron

First of all, faces $V_1V_2V_6V_5$, $V_1V_4V_8V_5$ and $V_1V_2V_3V_4$ are split into triangles by diagonal lines V_1V_6, V_1V_8 and V_1V_3, respectively. According to the number of diagonal lines going through node V_7, which depends on the identifier of nodes on the faces $V_2V_3V_7V_6$, $V_5V_6V_7V_8$ and $V_4V_3V_7V_8$, there exist eight

subdivision possibilities. See Fig. 5(a) where no diagonal line going through V_7, see Fig. 5(b) where three diagonal lines going through V_7, see Fig. 5(c)-5(e) where for each case one diagonal line going through V_7, and see Fig. 5(f)-5(h) where for each case two diagonal lines going through V_7.

The subdivision results for all eight cases are listed in Table 3.

Cases	Subdivisions
Fig. 5(a)	$V_1V_2V_3V_6$, $V_1V_3V_6V_8$, $V_3V_6V_7V_8$, $V_1V_5V_6V_8$, $V_1V_3V_4V_8$
Fig. 5(b)	$V_1V_2V_3V_7$, $V_1V_2V_6V_7$, $V_1V_5V_6V_7$, $V_1V_5V_7V_8$, $V_1V_4V_7V_8$, $V_1V_3V_4V_7$
Fig. 5(c)	$V_1V_2V_3V_6$, $V_1V_3V_6V_7$, $V_1V_3V_4V_7$, $V_1V_5V_6V_8$, $V_1V_6V_7V_8$, $V_1V_4V_7V_8$
Fig. 5(d)	$V_1V_3V_6V_7$, $V_1V_5V_6V_7$, $V_1V_2V_3V_6$, $V_1V_5V_7V_8$, $V_1V_3V_7V_8$, $V_1V_3V_4V_8$
Fig. 5(e)	$V_1V_5V_6V_8$, $V_1V_6V_7V_8$, $V_1V_2V_6V_7$, $V_1V_2V_3V_7$, $V_1V_3V_7V_8$, $V_1V_3V_4V_8$
Fig. 5(f)	$V_1V_5V_6V_7$, $V_1V_3V_6V_7$, $V_1V_2V_3V_6$, $V_1V_5V_7V_8$, $V_1V_4V_7V_8$, $V_1V_3V_4V_7$
Fig. 5(g)	$V_1V_5V_6V_7$, $V_1V_2V_6V_7$, $V_1V_2V_3V_7$, $V_1V_5V_7V_8$, $V_1V_3V_4V_8$, $V_1V_3V_7V_8$
Fig. 5(h)	$V_1V_2V_6V_7$, $V_1V_2V_3V_7$, $V_1V_3V_4V_7$, $V_1V_5V_6V_8$, $V_1V_6V_7V_8$, $V_1V_4V_7V_8$

Table 3: Subdivisions of a hexahedra.

It is easy to see, the above described conforming subdivision is performed on each element locally, without any communication with its neighbouring elements. For a more sophisticated implementation, we refer to [2].

2.2. The finite element space of the P_1 element on the subdivided tetrahedral mesh

Let $\mathcal{T}_h$ be the conforming subdivision of the original hybrid mesh for the domain Ω using the above described method. On each element $T \in \mathcal{T}_h$, let φ denote the standard nodal basis function of the P_1 element on T associated with the node x. Then the finite element space of the P_1 element on $\mathcal{T}_h$ is constructed by a span of the local basis functions on each element T, i.e.,

$$V_h^T = \{v \in C(\overline{\Omega}) : v|_T \in \Phi_T, \forall T \in \mathcal{T}_h\}, \tag{1}$$

where

$$\Phi_T = \text{span}\{\varphi : T \in \mathcal{T}_h\}.$$

Let $H^1(\Omega)$ and $L^2(\Omega)$ denote the standard Sobolev and Lebesgue spaces (see [1]) on Ω, respectively. Let h denote the discretized mesh parameter. Under the assumption that the subdivided tetrahedral mesh is regular, we have the following approximation properties for the standard P_1 element on the tetrahedral mesh:

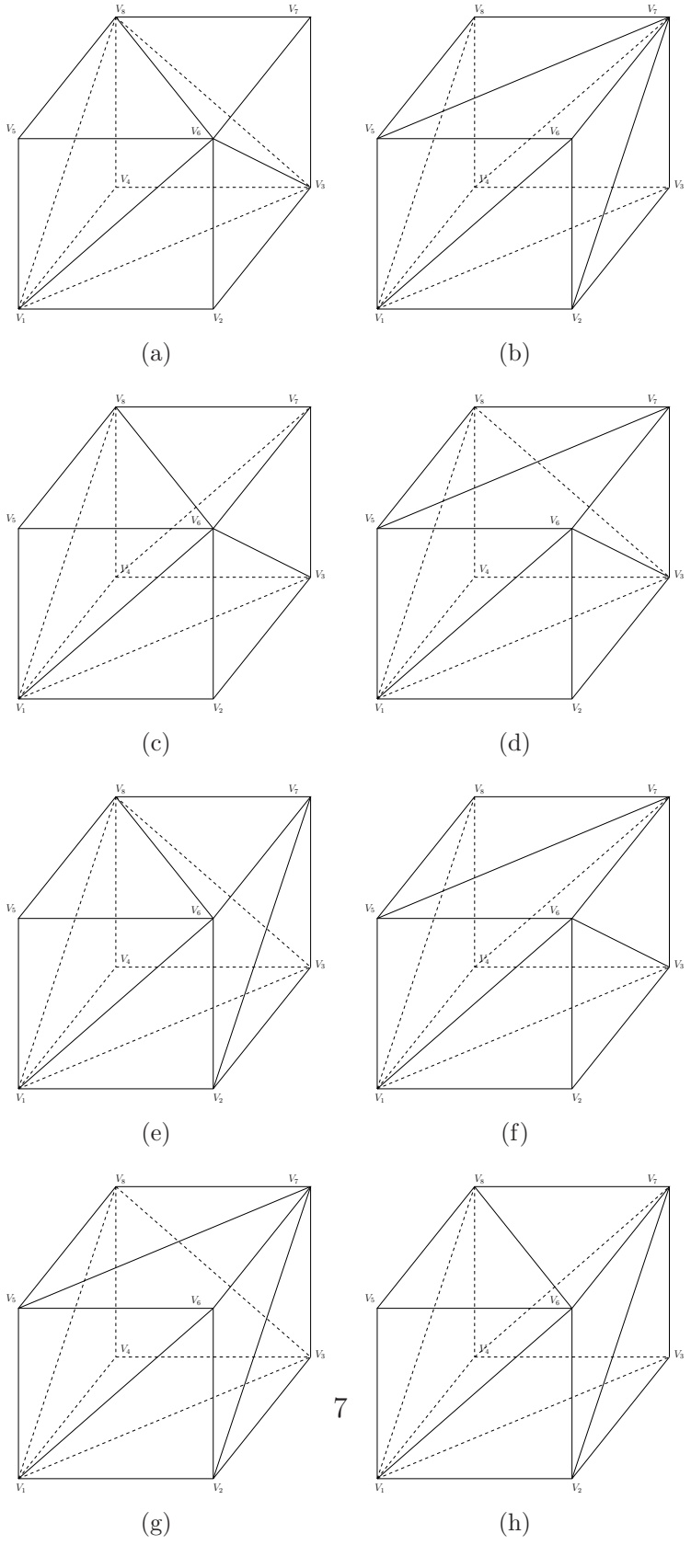

Figure 5: A schematic representation of subdivisions of a hexahedron into tetrahedra.

Theorem 1. 1. *There is an interpolation operator* $I_C^T\colon L^2(\Omega) \longrightarrow V_h^T$ *such that*

$$\|v - I_C^T v\|_{L^2(\Omega)} \leq c\,|v|_{L^2(\Omega)} \quad \textit{for all } v \in L^2(\Omega),$$

and

$$\|v - I_C^T v\|_{L^2(\Omega)} + h|v - I_C^T v|_{H^1(\Omega)} \leq c\,h\,|v|_{H^1(\Omega)} \quad \textit{for all } v \in H^1(\Omega)$$

with a mesh-independent constant c.

2. *There is an interpolation operator* $I_L^T\colon H^2(\Omega) \longrightarrow V_h^T$ *such that*

$$\|v - I_L^T v\|_{L^2(\Omega)} + h|v - I_L^T v|_{H^1(\Omega)} \leq c\,h^2\,|v|_{H^2(\Omega)} \quad \textit{for all } v \in H^2(\Omega)$$

with a mesh-independent constant c.

The operators I_C^T and I_L^T are the Clément-type interpolation operator and the Lagrange-type interpolation operator, respectively. See e.g. [3].

3. The extended linear finite element on a hybrid mesh

The second approach is to keep the topology of the hybrid mesh, but extend the standard P_1 element on such a mesh in an algebraic way.

3.1. Conforming subdivision of a hybrid mesh with additional nodes

First, let $\mathcal{T}_h'$ be the admissible subdivision of $\mathcal{M}_h$ into tetrahedra, obtained in the following way: we add nodes at the centers of quadrilateral faces and subdivide each of them into four triangles, then add a node at the center of the element, and finally connect this center node with all the original nodes and the face center nodes.

By this means, a pyramid is split into eight tetrahedra, a prism into fourteen tetrahedra and a hexahedra into twenty-four tetrahedra, see Fig. 6 for an illustration. One easily sees that such a subdivision results in an admissible refinement $\mathcal{T}_h'$ of the original hybrid mesh $\mathcal{M}_h$. So it leads to a conforming mesh with additional nodes, i.e. introducing new nodal degrees of freedom which will be eliminated in the next step.

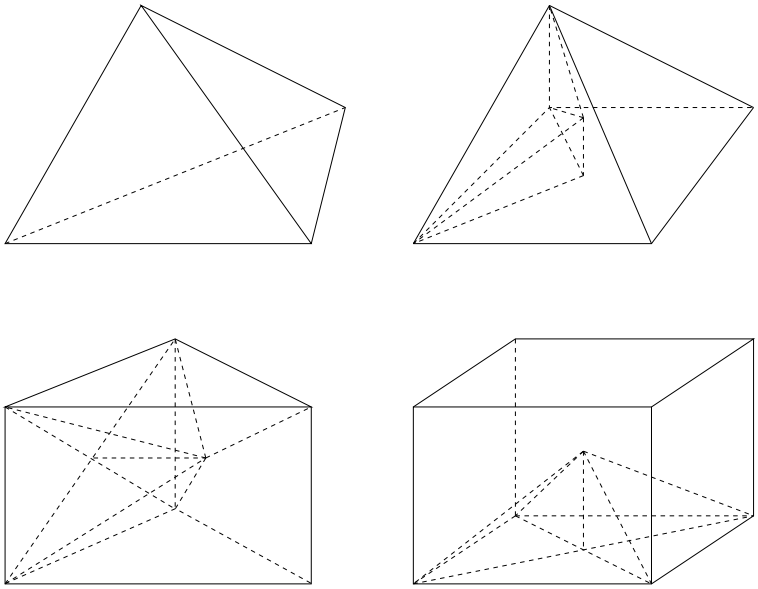

Figure 6: Splitting of hybrid elements into tetrahedra with added nodes.

3.2. The finite element space of the extended linear element

For constructing the extended linear element on $\mathcal{M}_h$, we firstly consider a nodal basis function on an element M from $\mathcal{M}_h$ as follows: Let x be a node of M, let x_{F_i}, $i = 1, ...,$ denote the center node of those non-triangular faces F_i which contain x as a node, and let x_M denote the center node of M.

As our finite element space on the hybrid mesh $\mathcal{M}_h$ we first take the standard P_1 finite element space on the underlying tetrahedral mesh $\mathcal{T}_h'$ and then replace the degrees of freedom associated to the added nodes by averaging over neighboring nodes of the original mesh. Thus it keeps the same number of nodal degrees of freedom as the number of original nodes of the hybrid mesh.

Then on the element M, the nodal basis function φ associated with the node x is given by

$$\varphi = \hat{\varphi} + \sum_i \frac{1}{N_{F_i}} \hat{\varphi}_{F_i} + \frac{1}{N_M} \hat{\varphi}_M \ , \tag{2}$$

where $\hat{\varphi}$, $\hat{\varphi}_{F_i}$, and $\hat{\varphi}_M$ denote the nodal basis functions of the P_1 element on the subdivision of M associated with the nodes x, x_{F_i} and x_M, respectively,

and N_{F_i} and N_M are the numbers of nodes of the face F_i and the element M, respectively. It is easy to see that such a constructed piece-wise linear basis function has larger support compared to a standard linear basis function.

Then the finite element space of the extended linear element on $\mathcal{M}_h$ is constructed by a span of the local basis functions on each element M, i.e.,

$$V_h^M = \{v \in C(\overline{\Omega}) : v|_M \in \Phi_M, \forall M \in \mathcal{M}_h\}, \tag{3}$$

where

$$\Phi_M = \text{span}\{\varphi : M \in \mathcal{M}_h\}.$$

One easily sees that the extended linear element is an $H^1(\Omega)$-conforming finite element and the following approximation properties as the standard P_1 element on tetrahedral meshes hold:

Theorem 2. 1. *There is an interpolation operator* $I_C^M \colon L^2(\Omega) \longrightarrow V_h^M$ *such that*

$$\|v - I_C^M v\|_{L^2(\Omega)} \leq c\,|v|_{L^2(\Omega)} \quad \textit{for all } v \in L^2(\Omega),$$

and

$$\|v - I_C^M v\|_{L^2(\Omega)} + h|v - I_C^M v|_{H^1(\Omega)} \leq c\,h\,|v|_{H^1(\Omega)} \quad \textit{for all } v \in H^1(\Omega)$$

with a mesh-independent constant c.

2. *There is an interpolation operator* $I_L^M \colon H^2(\Omega) \longrightarrow V_h^M$ *such that*

$$\|v - I_L^M v\|_{L^2(\Omega)} + h|v - I_L^M v|_{H^1(\Omega)} \leq c\,h^2\,|v|_{H^2(\Omega)} \quad \textit{for all } v \in H^1(\Omega)$$

with a mesh-independent constant c.

The operators I_C^M and I_L^M are the Clément-type interpolation operator and the Lagrange-type interpolation operator, respectively. For details, see [8, 11].

Compared with the first finite element method, the second one is more expensive although its conforming subdivision is easier to realize: it produces much more tetrahedra and the extended linear basis function has much larger support. Thus in computation, the first finite element method will be faster than the second one due to the less costly finite element assembly procedure. However, for hybrid meshes containing arbitrary types of polyhedral elements, the second finite element method might be easier to adapt.

4. Applications on the fluid-structure interaction problem

In [10, 11, 9], the second finite element method has been applied to the FSI problem on hybrid meshes, where the partitioned Newton and partitioned Robin-Neumann preconditioned GMRES algorithms are used to solve the FSI problem for the outer iteration, and for the inner iteration, extended versions of special algebraic multigrid (AMG) methods ([7, 6]) are used to solve the fluid and structure sub-problems discretized by this particular finite element method. We refer to [9, 11] for details of numerical results.

The aim of this note is to compare numerical solutions of the FSI problem and the performance using these two finite element methods on hybrid meshes. Thus we take the same FSI benchmark as the one from [9, 11], i.e. we use the same computational domain (a cylinder), the same hybrid meshes, the same FSI solvers, the same AMG solvers, etc., except that we use these two finite element methods to discretize both sub-problems.

4.1. Subdivision of the hybrid meshes for the first finite element method

Hybrid meshes are generated for the fluid and the structure domains with matching nodes at the common interface (see [5]). Two meshes are used for simulations, see Fig. 7. The coarse hybrid mesh contains $4,176$ nodes and

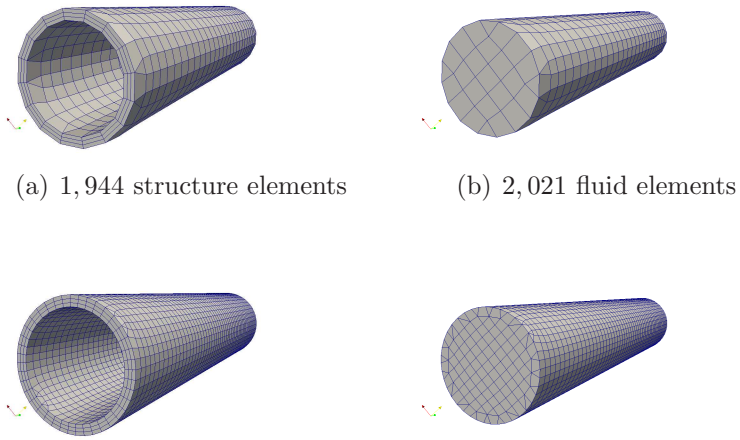

(a) $1,944$ structure elements (b) $2,021$ fluid elements

(c) $7,434$ structure elements (d) $10,055$ fluid elements

Figure 7: Two meshes for the FSI computational domain: Coarse mesh (first row) and fine mesh (second row).

3, 965 elements (1, 944 structure elements and 2, 021 fluid elements), and the fine hybrid mesh contains 17, 904 nodes and 17, 489 elements (7, 434 structure elements and 10, 055 fluid elements). The overall degrees of freedom for these two meshes are about 16, 000 and 70, 000, respectively.

For the first finite element method, we need to make a conforming subdivision of each hybrid mesh without adding new nodes. See Fig. 8. The resulting coarse tetrahedral mesh includes 22, 474 elements (11, 520 structure elements and 10, 954 fluid elements), and the resulting fine tetrahedral mesh includes 98, 158 elements (44, 388 structure elements and 53, 770 fluid elements).

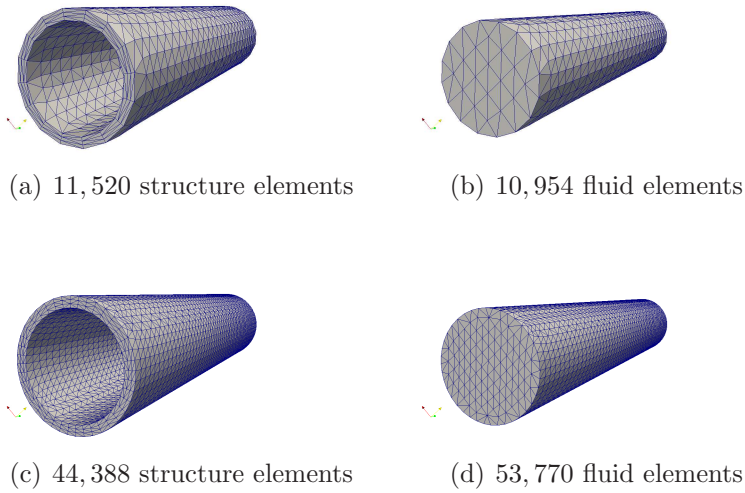

(a) 11, 520 structure elements (b) 10, 954 fluid elements

(c) 44, 388 structure elements (d) 53, 770 fluid elements

Figure 8: Two tetrahedral meshes subdivided from the hybrid meshes for the FSI computational domain: Coarse mesh (first row) and fine mesh (second row).

It is easy to see the subdivision of the original hybrid meshes into pure tetrahedral meshes produces about six times as many tetrahedral elements as the original hybrid elements. This is due to the fact that most of elements in these two hybrid meshes are hexahedron. On the other hand, recall that for the second finite element method, each non-tetrahedral element is subdivided according to Section 2.1. Thus the subdivision for the second finite element produces about twenty-four times as many tetrahedral elements as the original hybrid elements.

Note in principle, that it is not required to generate the subdivision ex-

plictly for both finite element methods. The finite element assembly is performed element-wise on the original hybrid mesh, with special care of the corresponding subdivision of each non-tetrahedral element.

4.2. Comparison of the numerical solutions

For these two finite element methods on hybrid meshes, we compare the numerical solutions of the pressure wave propagations along the center line of the computational domain for different time levels. We choose the time step size $\Delta t = 0.125$ ms. The results are plotted in Fig. 9 for the coarse mesh , and in Fig. 10 for the fine mesh.

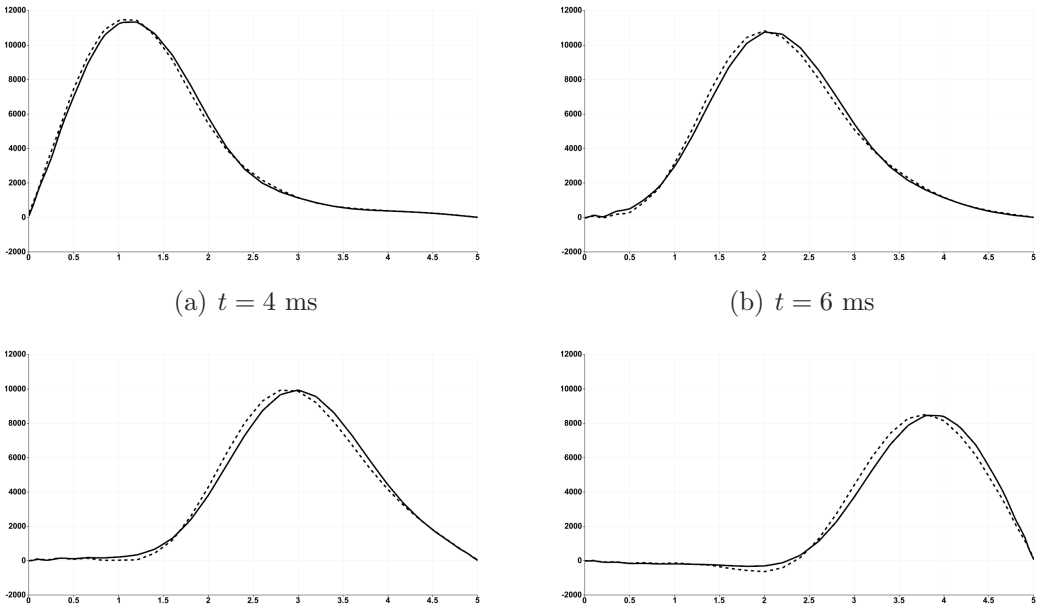

(a) $t = 4$ ms (b) $t = 6$ ms

(c) $t = 8$ ms (d) $t = 10$ ms

Figure 9: Pressure waves on the coarse mesh at different time levels with a time step size: $\Delta t = 0.125$ ms. The horizontal axis represents the centerline of the cylinder; the pressure is plotted in the vertical direction. The solid lines represent the solutions with the first finite element method; the dashed lines represent the solutions with the second finite element method.

As expected, on both meshes, the numerical results from these two finite element methods are almost identical to each other.

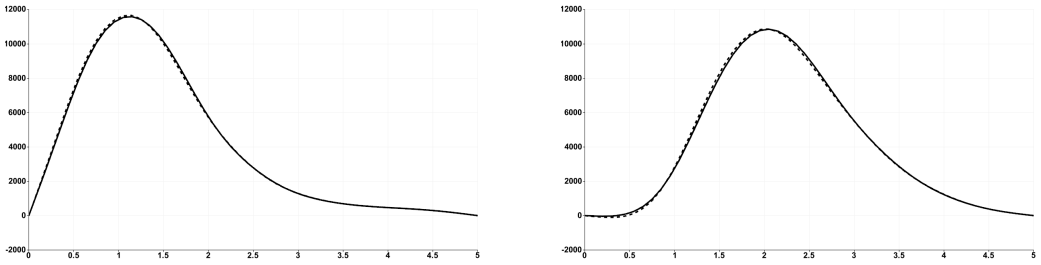

(a) $t = 4$ ms

(b) $t = 6$ ms

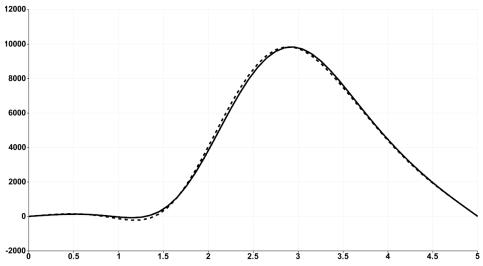

(c) $t = 8$ ms

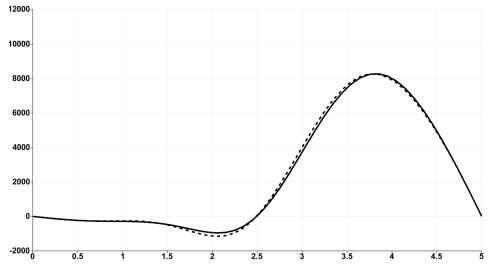

(d) $t = 10$ ms

Figure 10: Pressure waves on fine mesh at different time levels with a time step size: $\Delta t = 0.125$ ms. The horizontal axis represents the centerline of the cylinder; the pressure is plotted in the vertical direction. The solid lines represent the solutions with the first finite element method; the dashed lines represent the solutions with the second finite element method.

4.3. Comparison of the performance

For measuring the performance, the code is tested on a laptop with an Intel Core of 2.67 GHz and 4 GB memory. We solve the FSI problem with the Robin-Neumann preconditioned GMRES solver (see [9]) and the Newton based solver (see [11]), respectively, each of which is performed on the coarse and fine meshes. On each mesh, we compare the CPU time in seconds for the cost of one time step using these two finite element methods (FEMs): the first finite element method (I) and the second finite element method (II). We choose time step sizes $\Delta t = 0.0625, 0.125, 0.25, 0.5$ ms.

See the cost in Table 4. As excepted, the first finite element method (I) is much more efficient than the second one (II) for all these test cases due to its faster finite element assembly procedure. For each finite element method, as was already observed in [9], that the cost of one time step is independent of the time step size for both solvers, and the RN preconditioned GMRES

FSI solvers	RN-GMRES				Newton			
Meshes	Coarse		Fine		Coarse		Fine	
FEMs	I	II	I	II	I	II	I	II
0.0625 ms	31 s	249 s	355 s	4751 s	168 s	811 s	1532 s	14707 s
0.125 ms	28 s	242 s	331 s	4719 s	165 s	815 s	1505 s	14645 s
0.25 ms	33 s	249 s	360 s	4753 s	164 s	817 s	1452 s	14553 s
0.5 ms	33 s	250 s	363 s	4752 s	152 s	811 s	1935 s	19468 s

Table 4: Comparison of cost for solving the FSI problem at one time step using two finite element methods (I and II) on hybrid meshes.

solver is more efficient than the Newton based solver.

5. Conclusions

In this note, we construct a P_1 finite element on the conforming subdivision of hybrid meshes, which is compared with our previously extended linear finite element on such meshes in the FSI applications. It turns out to be more efficient than the previous one. Thus it is considered as a good alternative of the finite element discretization for the FSI problem developed in [8].

References

[1] R. A. Adams and J. J. F. Fournier. *Sobolev Spaces*, volume 140 of *Pure and Applied Mathematics*. Academic Press, Amsterdam, Boston, second edition, 2003.

[2] Prsent Au, Julien Dompierre, Paul Labbé, Marie gabrielle Vallet, and Ricardo Camarero. How to subdivide pyramids, prisms and hexahedra into tetrahedra, 1999.

[3] D. Braess. *Finite Elements. Theory, fast solvers, and applications in solid mechanics*. Springer, Berlin, Heidelberg, New York, 2nd edition, 2001.

[4] Y. Kallinderis and . T. Ahn. Incompressible Navier-Stokes method with general hybrid meshes. *Journal of Computational Physics*, 210:75–108, 2005.

[5] F. Kickinger. Website. `http://www.meshing.org/`.

[6] F. Kickinger. Algebraic multigrid for discrete elliptic second-order problems. In *Multigrid Methods V. Proceedings of the 5th European Multigrid conference (ed. by W. Hackbush), Lecture Notes in Computational Sciences and Engineering, vol. 3*, pages 157–172. Springer, 1998.

[7] M. Wabro. Coupled algebraic multigrid methods for the oseen problem. *Comput. Vis. Sci.*, 7:141–151, 2004.

[8] H. Yang. *Numerical Simulation of Fluid-Structure Interaction Problems on Hybrid Meshes with Algebraic Multigrid Methods*. PhD thesis, Johannes Kepler University Linz, 2010.

[9] H. Yang. A numerical study on a preconditioned GMRES solver with algebraic multigrid accelerations for the fluid-structure interaction problems on hybrid meshes. Ricam Report 2011-15, Johann Radon Institute for Computational and Applied Mathematics (RICAM), 2011. submitted.

[10] H. Yang and W. Zulehner. A Newton based fluid-structure interaction solver with algebraic multigrid methods on hybrid meshes. In Y. Huang, R. Kornhuber, O. Widlund, and J. Xu, editors, *Domain Decomposition Methods in Science and Engineering*, pages 285–292. Springer, 2011.

[11] H. Yang and W. Zulehner. Numerical simulation of fluid-structure interaction problems on hybrid meshes with algebraic multigrid methods. *Journal of Computational and Applied Mathematics*, 235:5367–5379, 2011.